The Astrophysical Journal Supplement Series, 286:7 (12pp), 2026 September https://doi.org/10.3847/1538-4365/ae8795

Multiband Optical Photometric Variability of the Blazar OJ 287 from 2015 to 2025

Alok C. Gupta[1,2,3], Karan Dogra[2], Mark Kidger[4,5,6], Mauri J. Valtonen[7,8], Paul J. Wiita[9], Pankaj Kushwaha[10], Sergey S. Savchenko[11], Sofia O. Kurtanidze[3,12], Svetlana G. Jorstad[11,13], Alan P. Marscher[13], Katsura Matsumoto[14], Lang Cui[1], Shao Ming Hu[15], Goran Damljanovic[16], Rumen Bachev[17], O. Vince[16], Mai Liao[18], Zhongxiang Wang[19], A. Darriba[20,21,22], S. Haque[23], F. S. Alfaro[22], J. B. Amatller[22], J. M. F. Andujar[22], S. Arnold[24], T. Arranz[22], M. Bachini[22], C. L. Barcelo[22], S. Boeva[17], G. A. Borman[25], D. Boyd[26], D. Buczinski[27], J. D. Casal[22], X. Chen[15], J. M. Cores[22], F. C. Cucarella[22], P. U. Devanand[2], V. Dhiman[2], L. T. Espasa[22], J. H. Fan[28], R. G. Farfan[22], J. R. Fernandez[22], F. Garcia[22], R. C. García[22], H. Gaur[2], J. C. Gomez[22], J. L. S. Gonzalez[22], J. L. Gonzalez-Carballo[22], T. S. Grishina[11], F. H. Grondona[22], M. F. Gu[29], H. Guo[29], V. A. Hagen-Thorn[11], G. Hurst[30], S. Ibryamov[31], R. Z. Ivanidze[3], N. James[32], B. Jardine[23], S. Johnstone[33], M. D. Jovanovic[16], N. Kalita[34], S. Karge[35], S. Kishore[2,36], E. N. Kopatskaya[11], O. M. Kurtanidze[3,12,37], A. Kurtenkov[17,38], E. G. Larionova[11], E. R. Lorenz[22], J. Lozano[22], E. F. Mananes[22], F. L. Martínez[22], M. Mobberley[39], M. Morales-Aimar[22], D. A. Morozova[11], M. G. Nikolashvili[3,12], Y. Nikolov[17], R. N. Nogues[22], P. A. Novikova[40], L. M. Penas[22], A. E. Perez[22], C. Perello[22], R. Pickard[24,49], F. G. Pinilla[22], G. Poyner[41], F. Rahmatullaeva[42], B. Rajkumar[23], N. G. Ribes[22], E. Semkov[17,49], E. V. Shishkina[11], M. Stojanovic[16], A. Strigachev[17], T. Tripathi[2], Yu. V. Troitskaya[11], I. S. Troitskiy[11], J. Valero[22], A. A. Vasilyev[11], B. Villarroel[43], A. E. Volvach[44], L. N. Volvach[44], S. J. Wagner[45], Z. R. Weaver[13], Wen-Xin Yang[28], Z. Zhang[46], A. V. Zhovtan[25], W. Zuo[29], N. Kojiguchi[47], and Y. Sugiura[48]

[1] Xinjiang Astronomical Observatory, Chinese Academy of Sciences, 150 Science 1-Street, Urumqi 830011, People's Republic of China; acgupta30@gmail.com, cuilang@xao.ac.cn
[2] Aryabhatta Research Institute of Observational Sciences (ARIES), Manora Peak, Nainital 263001, India; karandogra987@gmail.com
[3] Abastumani Observatory, Mt. Kanobili, 0301 Abastumani, Georgia
[4] European Space Astronomy Centre, European Space Agency, E-28691 Villanueva de la Cañada, Madrid, Spain
[5] Variable Star Section, British Astronomical Association, Villanueva del Pardillo, 28229 Madrid, Spain
[6] Observadores de Supernovas (ObSN), Villanueva del Pardillo, 28229 Madrid, Spain
[7] FINCA, University of Turku, Turku, Finland
[8] Department of Physics and Astronomy, University of Turku, Turku, Finland
[9] Department of Physics, The College of New Jersey, 2000 Pennington Road, Ewing, NJ 08628-0718, USA
[10] Department of Physical Sciences, IISER Mohali, Knowledge City, Sector 81, Manauli PO SAS Nagar, Punjab 140306, India
[11] St. Petersburg State University, 7/9, Universitetskaya nab., 199034, St. Petersburg, Russia
[12] Landessternwarte, Zentrum für Astronomie der Universität Heidelberg, Königstuhl 12, 69117 Heidelberg, Germany
[13] Institute for Astrophysical Research, Boston University, 725 Commonwealth Avenue, Boston, MA 02215, USA
[14] Astronomical Institute, Osaka Kyoiku University, Osaka 582-8582, Japan
[15] Shandong Key Laboratory of Space Environment and Exploration Technology, School of Space Science and Technology, Institute of Space Sciences, Shandong University, Weihai, Shandong 264209, People's Republic of China
[16] Astronomical Observatory, Volgina 7, 11060 Belgrade, Serbia
[17] Institute of Astronomy and National Astronomical Observatory, Bulgarian Academy of Sciences, 72 Tsarigradsko Shosse Boulevard, 1784 Sofia, Bulgaria
[18] Instituto de Estudios Astrofisicos, Facultad de Ingenieria y Ciencias, Universidad Diego Portales, Av. Ejército 441, Santiago, Chile
[19] Department of Astronomy, School of Physics and Astronomy, Key Laboratory of Astroparticle Physics of Yunnan Province, Yunnan University, Kunming 650091, People's Republic of China
[20] American Association of Variable Star Observers (AAVSO), 49 Bay State Road, Cambridge, MA 02138, USA
[21] Group M1, Centro Astronómico de Avila, Madrid, Spain
[22] Supernova Observers (ObSN), Paseo Condes de Barcelona 3, 06010 Badajoz, Spain
[23] Department of Physics, The University of the West Indies, St. Augustine, Trinidad and Tobago
[24] Variable Star Section, British Astronomical Association, PO Box 702, Tonbridge TN9 9TX, UK
[25] Crimean Astrophysical Observatory RAS, P/O Nauchny, 298409, Russia[†]
[26] Variable Star Section, British Astronomical Association, 5 Silver Lane, West Challow, Wantage, Oxon, OX12 9TX, UK
[27] Variable Star Section, British Astronomical Association, Templecroft, Tarbatness Road, Portmahomack, Near Tain, Ross-shire IV20 1RD, UK
[28] Center for Astrophysics, Guangzhou University, Guangzhou 510006, People's Republic of China
[29] Shanghai Astronomical Observatory, Chinese Academy of Sciences, 80 Nandan Road, Shanghai 200030, People's Republic of China
[30] Variable Star Section, British Astronomical Association, 16 Westminster Close, Basingstoke, Hampshire RG22 4PP, UK
[31] Department of Physics and Astronomy, University of Shumen, 115, Universitetska Str., 9700 Shumen, Bulgaria
[32] Variable Star Section, British Astronomical Association, 11 Tavistock Road, Chelmsford, Essex CM1 6JL, UK
[33] Variable Star Section, British Astronomical Association, Warrington, Cheshire, UK
[34] Polar Research Institute of China, 451 Jinqiao Road, Shanghai 200129, People's Republic of China
[35] Die Bundesdeutsche Arbeitsgemeinschaft für Veränderliche Sterne, Munsterdamm 90, 12169 Berlin, Germany
[36] Indian Institute of Astrophysics (IIA), 2nd Block, Koramangala, Bangalore 560 034, India
[37] Engelhardt Astronomical Observatory, Kazan Federal University, Tatarstan, Russia
[38] Faculty of Physics, Sofia University "St. Kliment Ohridski", 5 James Bourchier Boulevard, 1164 Sofia, Bulgaria
[39] Variable Star Section, British Astronomical Association, Denmara, 5 Old Hall Lane, Cockfield, Bury St Edmunds, Suffolk IP30 0LQ, UK
[40] Scuola Normale Superiore, Piazza dei Cavalieri 7, Pisa, 56126, Italy
[41] Variable Star Section, British Astronomical Association, Kingstanding, Birmingham, UK
[42] Institute of Astrophysics, National Academy of Sciences of Tajikistan, Str. Ayni 299/5, Dushanbe, 704063, Tajikistan
[43] Nordita, KTH Royal Institute of Technology and Stockholm University, Hannes Alfvéns väg 12, SE-106 91 Stockholm, Sweden
[44] Radio Astronomy Laboratory of Crimean Astrophysical Observatory, Katsively, RT-22, Crimea[†]
[45] Landessternwarte, Universität Heidelberg, Königstuhl, 69117 Heidelberg, Germany
[46] Shanghai Astronomical Observatory, Key Laboratory of Radio Astronomy, Chinese Academy of Sciences, Shanghai 200030, People's Republic of China
[47] Okayama Observatory, Kyoto University, Okayama 719-0232, Japan

[48] Toyohashi Audio-visual Education Center, Toyohashi, Aichi 441-3147, Japan

Received 2026 April 29; revised 2026 June 25; accepted 2026 July 6; published 2026 August 12

Abstract

We present the most densely sampled multiband optical photometric observations of the peculiar BL Lacertae object OJ 287 from 2015 to 2025 with a focus on its optical activity on diverse timescales. We present a total of 2296, 10,927, 11,484, and 2982 data points in *B*, *V*, *R*, and *I* bands, respectively. The densely sampled observations allow us to keep track of the source evolution that it has exhibited since the start of the predicted major optical flaring activity at the end of 2015. The study reveals clear and persistent bluer-when-brighter trends in both the long-term and short-term variations. Different bands were cross-correlated with discrete correlation functions, which peak at zero lag, implying cospatial emission. Using eight optical spectra in the low-flux states of OJ 287 taken from 2017 October 21 to 2017 November 22, from Steward Observatory, we estimate the central black hole mass to be at least $3.89 \times 10^9 M_\odot$ from the [O III] line width. The emission mechanism of the binary black hole blazar, and its possible implication in various aspects of multimessenger astronomy, are briefly discussed.

Unified Astronomy Thesaurus concepts: Quasars (1319); BL Lacertae objects (158); Active galaxies (17)

1. Introduction

Blazars are jetted active galactic nuclei (AGNs), which are traditionally designated as being radio-loud, with a large-scale, powerful, and relativistic jet of plasma directed nearly toward our line of sight. They are characterized by a strong and rapidly variable continuum that spans the entire accessible electromagnetic (EM) spectrum from radio to γ-rays (e.g., S. O. Brien & VERITAS Collaboration 2017; M. de Naurois 2021) with high and variable polarized radio and optical continua; some exhibit recently detected variable X-ray polarization too (e.g., L. Di Gesu et al. 2023; A. C. Gupta et al. 2023; R. Imazawa et al. 2023). The broadband multiwavelength (MW) continuum revealed a new characteristic feature of blazar emission—a broad bimodal spectral energy distribution (SED; G. Fossati et al. 1998; A. A. Abdo et al. 2010), primarily of nonthermal nature. Studies of these two humps are critical in investigations of the emission mechanisms and the underlying physical conditions (e.g., P. Kushwaha et al. 2018a, 2018b; S. Gao et al. 2019; E. Prandini & G. Ghisellini 2022; K. P. Singh et al. 2022; G. Harutyunyan et al. 2025; P. Kushwaha 2025; P. K. Navaneeth et al. 2025). Given the ubiquity of variations in all bands, these explorations are greatly facilitated by simultaneous broadband monitoring. The low-energy part of the SED emission, extending from radio up to X-rays, reaching a maximum between the infrared (IR) and X-ray bands is widely accepted to be the synchrotron emission from ultra-relativistic nonthermal electrons in the relativistic jet. The origin of the high-energy part of the SED is still unclear, as both leptonic and hadronic models reproduce it reasonably well within the available observational constraints. The leptonic emission scenarios attribute it to inverse-Compton scattering off the synchrotron emitting electrons of a combination of soft photon fields arising both within and external to the jet (e.g., K. P. Singh et al. 2022). The alternative hadronic scenarios reproduce this high-energy emission via proton synchrotron and/or cascades resulting from the interactions of relativistic protons with proton and photon fields (e.g., S. Gao et al. 2019).

Blazars are taken to be the combination of flat-spectrum radio quasars (FSRQs) and BL Lacertae (BL Lac) objects; both exhibit similar continuum behavior, with the primary difference being the optical spectrum. The former shows prominent broad-emission-line features, while in the latter, they are weak or these features are completely lacking. OJ 287 is a BL Lac–type blazar at a redshift of $z = 0.304$ (M. L. Sitko & V. T. Junkkarinen 1985; K. Nilsson et al. 2010). It is one of the best-monitored blazars with an extensive prediscovery light curve, obtained from archival plates and early postidentification observations driven by its enigmatic dynamic variability at optical and radio bands (M. L. Sitko & V. T. Junkkarinen 1985, and references therein). Subsequently, the identification of recurring optical outbursts at ~12 yr intervals led to the popular interpretation of the source as a binary supermassive black hole (SMBH) system, with recurring outbursts attributed to the impact of the secondary on the accretion disk of the primary (A. Sillanpaa et al. 1988; M. J. Valtonen et al. 2025, and references therein). The onset of the next set of flares, in 1994 and 1995, around the model-predicted schedule gave this hypothesis further credence and has driven substantial coordinated MW monitoring of OJ 287 (A. Sillanpaa et al. 1996a, 1996b). In its nearly regular cycle of outbursts, M. J. Valtonen et al. (2006) predicted that OJ 287 was due for another outburst season in 2006–2010. In an extensive optical photopolarimetric study of the source from 2005 to 2009, the predicted double-peaked outbursts were detected in 2005 December and 2007 December, and it was suggested that both the double-peaked bursts and the evolution of the optical polarization position angle could be explained as a sign of resonant accretion of magnetic field lines, a "magnetic breathing" of the disk (C. Villforth et al. 2010). The next predicted double-peaked outbursts were detected in 2015 December (M. J. Valtonen et al. 2016) and 2019 July (S. Laine et al. 2020). The 2019 July flare was detected using the Spitzer telescope, as the source was not available from ground-based optical/IR observations. OJ 287's MW behavior has been extensively observed since 2015 by various groups and the Multiwavelength Observations and Modeling of OJ 287 (MOMO) collaboration (e.g., G. Bhatta et al. 2016; M. J. Valtonen et al. 2016; A. Goyal et al. 2018; P. Kushwaha et al. 2018a, 2018b; S. Komossa et al. 2020, 2021a, 2021c, 2021b, 2023b; S. Laine et al. 2020; M. Pal et al. 2020; R. Prince et al. 2021; K. P. Singh

[49] Deceased.

† While the AAS journals adhere to and respect UN resolutions regarding the designations of territories (available at http://www.un.org/press/en), it is our policy to use the affiliations provided by our authors on published articles.

et al. 2022; S. Britzen et al. 2023; A. C. Gupta et al. 2023, and references therein). The other prominent interpretation of the recurrent flares attributes it to jet precession (e.g., S. Britzen et al. 2018, and references therein) and it still continues to be invoked (e.g., M. S. Butuzova & A. B. Pushkarev 2020), though these models primarily focus on explanation rather than prediction (e.g., see P. Kushwaha 2020 for a succinct summary of proposed models).

Despite the impact scenario binary-SMBH model being favored by current observational behavior, several aspects of the observations seem to be inconsistent with its predictions or claims. For example, the observed optical spectrum during flaring (e.g., H. Seta et al. 2009; A. C. Gupta et al. 2017; P. Kushwaha et al. 2018b) does not show a flat ($F_\nu \sim \nu^{0-0.2}$) spectrum, which is characteristic of the thermal bremsstrahlung emission that is claimed for the outbursts. Furthermore, neither an MW activity with a simultaneous flare of X-rays and γ-rays (P. Kushwaha et al. 2018b), nor a systematic large swing of optical polarization (A. C. Gupta et al. 2023), is expected during the flare in the case of the claimed thermal emission. Both of the latter behaviors indicate nonthermal broadband emission components. Additionally, the observed degree of optical polarization is still uncertain (e.g., H. Seta et al. 2009). Detection of both the expected impact-induced jet emission as well as the tidal accretion has been claimed (e.g., B. Giesers et al. 2018; S. Huang et al. 2021) and is also supported by previously available observations (N. Isobe et al. 2001, and references therein). However, the spectral nature is different (S. O. Brien & VERITAS Collaboration 2017; P. Kushwaha et al. 2018a, 2021) to the jet emission considered to be normal for the source (e.g., P. Kushwaha et al. 2013). Since most of the characteristic properties of the models are associated with the optical bands, multiband optical monitoring holds the key to addressing these issues, along with concurrent MW studies.

OJ 287 is monitored most thoroughly in optical bands, particularly *V* and *R*—the legacy EM window and the optical window are where the appearance of recurring outbursts is reported. Apart from the timing information, the polarization and spectral shape from multiband optical monitoring can provide the most crucial test of the model's spectrum, encoded in the color-flux variations (e.g., P. Kushwaha 2020; Gopal-Krishna 2024). Though the binary-impact-driven thermal flare is limited most likely to and around the expected recurrent flare, the rest of the activity is driven entirely by the jet—characterized by a nonthermal power-law spectrum, imprinted in the color variation that is a direct tracer of this and any additional spectral component (e.g., P. Kushwaha et al. 2018a). The color variability of blazars is often divided into two subcategories: bluer when brighter (BWB) and redder when brighter (RWB). The former is generally associated with BL Lac objects (M. F. Gu et al. 2006; Y.-H. Zhang et al. 2013; A. Wierzcholska et al. 2015), and the latter with FSRQs (C. M. Raiteri et al. 2008; E. Bonning et al. 2012). A recent study conducted by K. Dogra et al. (2025) revealed that the FSRQ 3C 454.3 follows an RWB trend up to a particular brightness value, after which the color behavior can be RWB, BWB, or achromatic. Nonetheless, some cases have been reported where the trends were interchanged (M. F. Gu & Y. L. Ai 2011) or the objects under study display achromatic behavior (C. M. Raiteri et al. 2023) instead. Most of the previous studies were done either on short timescales or did not have a sufficient number of observations to confidently constrain this behavior, which motivated us to study the long-term as well as short-term color behavior of OJ 287.

In this work, we present the most extensive and up-to-date study of the multiband optical flux and spectral variability of the source from 2015 September to 2025 April, the expected time of the onset of the first portions of an impact-model-predicted recurrent optical outburst (M. J. Valtonen et al. 2016). This is a continuation of our ongoing project on OJ 287 aimed at presenting a dense optical follow-up between the ∼12 yr optical outbursts in order to investigate and understand the behavior of this source and compare the emission with traits considered typical of the source and then allow us to make comparisons with proposed models (A. C. Gupta et al. 2017, 2019, 2022, 2023; P. Kushwaha et al. 2018a, 2018b, 2021; P. Kushwaha 2022; S. Kishore et al. 2024).

The present work is divided into six sections, with Section 2 briefly describing the optical observations and data reduction. In Section 3 we give the results of our multiband optical data analysis, with Section 4 explaining the black hole (BH) mass calculation, followed by a discussion in Section 5. We close with a summary of the findings in Section 6.

2. Multiband Optical Data

The multiband optical data collected under these campaigns is shown in Figure 1. The participating observatories, data collection periods, and other important information related to them are provided in Table 1. The image frames were first cleaned (e.g., using IRAF[50]), which involved bias correction, flat correction, and cosmic-ray removal, after which standard image reduction steps (e.g., using DAOPHOT II,[51] ESO-MIDAS,[52] and MAXIM-DL6,[53] etc.) were performed.

Once we have cleaned and reduced the raw science frames, differential photometry was performed to obtain *BVRI* magnitudes of OJ 287 using local standard stars 9, 12, and 13 in the blazar field (J. N. González-Pérez et al. 2001). Most observatories used the Johnson–Cousins broadband *BVRI* filters for photometric observations; however, some amateur observations were obtained using unfiltered (CV, i.e., clear/white light) measurements. These CV data were subsequently transformed to the equivalent Johnson–Cousins *V* band. All of the data were corrected for Galactic extinction with respective extinction values taken from NASA's extragalactic database. As data from multiple telescopes were available, we performed intercalibration between the different datasets. The offset between the light curves is calculated by identifying overlapping data points and then applying a mean shift, which sometimes is present (C. M. Raiteri et al. 2017a; MAGIC Collaboration et al. 2024). We found that the great majority of the offsets were well within the measurement uncertainties.

3. Variability Analysis

Figure 1 shows the optical flux behavior of OJ 287 between 2015 and 2025. Large-amplitude variations can be seen in all

[50] IRAF is distributed by the National Optical Astronomy Observatories, which are operated by the Association of Universities for Research in Astronomy, Inc., under a cooperative agreement with the National Science Foundation.

[51] Dominion Astronomical Observatory Photometry.

[52] European Southern Observatory—Munich Image Data Analysis System.

[53] CCD imaging and data reduction software by Diffraction Limited.

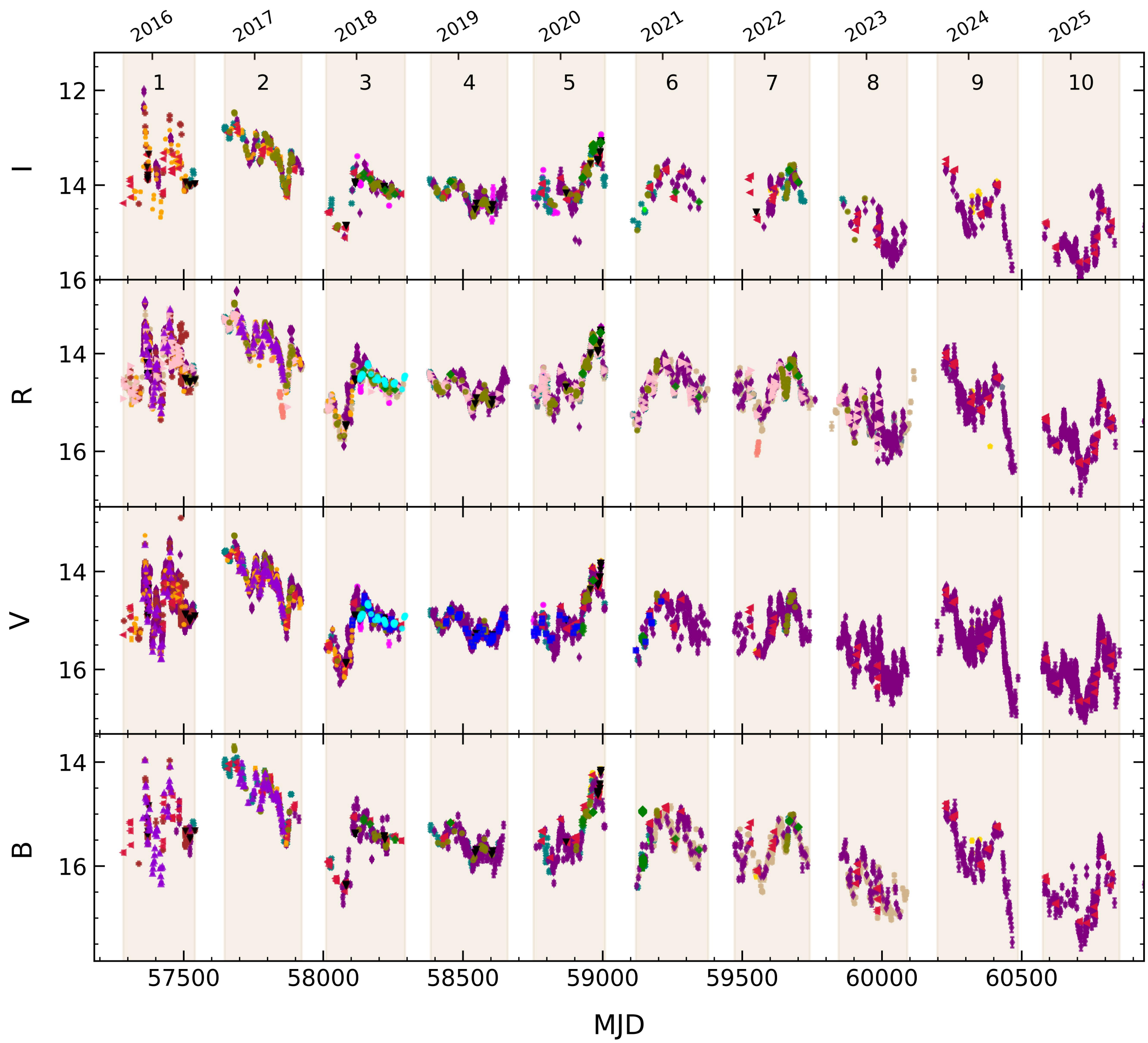

Figure 1. Multiband optical light curves of OJ 287 from 2015 to 2025. The *x*-axis and *y*-axis represent modified Julian date (MJD) and optical magnitudes, respectively. All four light curves are divided into 10 segments due to seasonal gaps. The observatories providing the data are indicated by the shapes and colors of the points as defined in Table 1.

four bands on similar timescales. As shown in Figure 1, the light curve across all four bands is divided into 10 segments (or observing seasons) due to yearly seasonal gaps with other gaps for individual observatories caused by weather, maintenance, etc. All segments, as well as the full light curve, have been used to better study the source's variability. As blazars show variability in the entire EM spectrum and over diverse timescales, we need to quantify these features as they can help to elucidate the emission mechanism along with the physical properties of the emission region. The variability amplitude is computed for all light-curve segments, the color–magnitude (CM) relationship is studied in detail, and the *Z*-transformed discrete correlation function is computed for all light-curve pairs in Sections 3.1, 3.2, and 3.3, respectively.

3.1. Variability Amplitude

One of the simplest ways to measure variation is the variability amplitude. It is related to the minimum ($m_{\rm min}$) and maximum ($m_{\rm max}$) reported magnitude within a given duration and the mean uncertainty of measurement (σ) as

$$V_{\rm amp} = \sqrt{(m_{\rm max} - m_{\rm min})^2 - 2\sigma^2}. \qquad (1)$$

The error associated with variability amplitude is given by

$$\Delta V_{\rm amp} = \sqrt{\frac{(m_{\rm max} - m_{\rm min})^2(\sigma_{\rm max}^2 + \sigma_{\rm min}^2) + 4\sigma^2\Delta\sigma^2}{V_{\rm amp}^2}}, \qquad (2)$$

Table 1
The Observatories, Data Collection Periods, and Other Relevant Details

Observatory/Observer	MJD Start	MJD Stop	Origin	Aperture (cm)	Filters	Data Points (N_{obs})	Marker	Color in Figure 1
Abastumani	58126.43	60430.26	Georgia	70	R	707	⬠	Slate gray
A. Darriba[a]	58103.55	59209.66	Spain	35.6	V	76	□	Blue
ARIES[b]	58562.15	59197.48	India	104/130	BVRI	11, 11, 11, 11	+	Lime
ASV[c]	58144.37	59700.35	Serbia	60/140	BVRI	86, 49, 83, 85	◇	Green
Belogradchik	58228.26	60414.33	Bulgaria	60	BVRI	55, 60, 60, 53	⬠	Gold
Crimean	57524.27	59863.59	Russia	70	BVRI	144, 158, 464, 204	✖	Teal
Mark Kidger[d]	57356.42	61139.82	International	Various	BVRI	1104, 9024, 5973, 1408	◇	Purple
Osaka	57295.29	60114.97	Japan	150	B	294	⬡	Tan
Perkins	60228.53	61030.44	United States	180	BVRI	285, 294, 166, 282	○	Crimson
Rozhen	57369.59	58993.30	Bulgaria	50/70/200	BVRI	53, 62, 85, 63	▽	Black
SATU[e]	57816.00	59558.00	West Indies	40	R	15	◯	Salmon
SMARTS[f]	57353.84	57857.55	Chile	130/150	BVR	111, 110, 111	△	Dark violet
St. Petersburg	57513.32	59938.62	Russia	40	BVRI	66, 80, 314, 202	◁	Olive
Steward[g]	58130.85	58292.65	United States	154/230	VR	34, 34	○	Cyan
Weihai	58121.27	58994.03	China	100	VRI	115, 121, 114	○	Magenta
Paper I[h]	57286.01	57529.48	International	Various	BVRI	40, 190, 437, 45	✚	Brown
Paper II[i]	57309.32	58103.82	International	Various	BVRI	46, 664, 840, 515	⋆	Orange
Paper III[j]	57284.00	59993.28	International	Various	R	1122	▷	Pink

Notes.
[a] Observatorio Astronomico Las Casqueras.
[b] Aryabhatta Research Institute of Observational Sciences.
[c] Astronomical station Vidojevica.
[d] Multiple telescopes.
[e] St. Augustine—Tuorla Observatory, Trinidad and Tobago.
[f] Small and Medium Aperture Research Telescope System.
[g] Steward Observatory Support of the Fermi Mission with 154 cm Kuiper and 230 cm Bok telescopes (P. S. Smith et al. 2009).
[h] A. C. Gupta et al. (2017).
[i] A. C. Gupta et al. (2019).
[j] A. C. Gupta et al. (2023).

where σ_{max}, σ_{min}, and $\Delta\sigma$ are the uncertainties in m_{max}, m_{min}, and σ. In order to have a proper track of how light-curve variability varied over time, V_{amp} has been calculated for all the light-curve segments and bands, with the results given in Table 2.

3.2. Flux and Color Variability

Closely related to flux variability is color variability, often called the CM relation, which can hint at possible physical processes mainly in the jet of the blazar. To study the color variability, we plotted the $B-$R and $V-R$ colors against the B and R magnitudes, respectively, as CM diagrams in Figure 2. We chose $B-$R and $V-R$ to plot differences between widely separated and close bands, respectively, as they have the largest number of color indices. To clearly track each segment's contribution in the CM diagrams, the segments are color coded. Although a blazar's spectral energy distribution is dominated by nonthermal emission, imprints of quasi-thermal emission can also be noted, at least in the quiescent/low state of the object under study.

Apparently, an overall linear trend is evident in Figure 2 throughout the observation campaign and across all segments. To quantify this behavior, we performed linear fits, with their respective slopes, intercepts, Pearson coefficients, r, and Spearman correlation coefficients, ρ, given in Table 3. We obtained 1425 $B-R$ color indices and 2110 $V-R$ color indices, with averages of 0.934 and 0.393, respectively. As can be seen in Figure 2, the BWB trend becomes more evident as the difference in color between bands increases. Apart from CM variations, color versus MJD variations have also been studied, as shown in Figure 3, which reveals a slow variation over the observing seasons fitted using a cubic polynomial of the form $ax^3 + bx^2 + cx + d$. For $B-R$ versus MJD, $a = -0.059 \pm 0.002$, $b = 0.040 \pm 0.002$, $c = 0.106 \pm 0.006$, and $d = 0.809 \pm 0.004$, whereas for $V-R$ versus MJD, $a = -0.044 \pm 0.002$, $b = 0.040 \pm 0.002$, $c = 0.074 \pm 0.004$, and $d = 0.367 \pm 0.003$. Although the long-term color versus Julian Date plot shows slow variation fitted using a cubic polynomial, the segment-wise color versus Julian Date variations are comparatively fast, although no definite trend is detected. Similarly to the CM plots, the color versus MJD trend becomes more evident for the more widely separated bands.

3.3. Z-transformed Discrete Correlation Function

To estimate the cross correlation between these unevenly sampled time series, we employ the z-transformed discrete correlation function (ZDCF), originally introduced by T. Alexander (1997). The ZDCF is an improvement over the discrete correlation function (DCF) developed by R. A. Edelson & J. H. Krolik (1988), addressing its statistical limitations by implementing two key modifications: equal-population binning and Fisher's z-transformation of the correlation coefficients. Unlike the traditional DCF, which bins time-lag pairs by fixed width, the ZDCF uses bins with

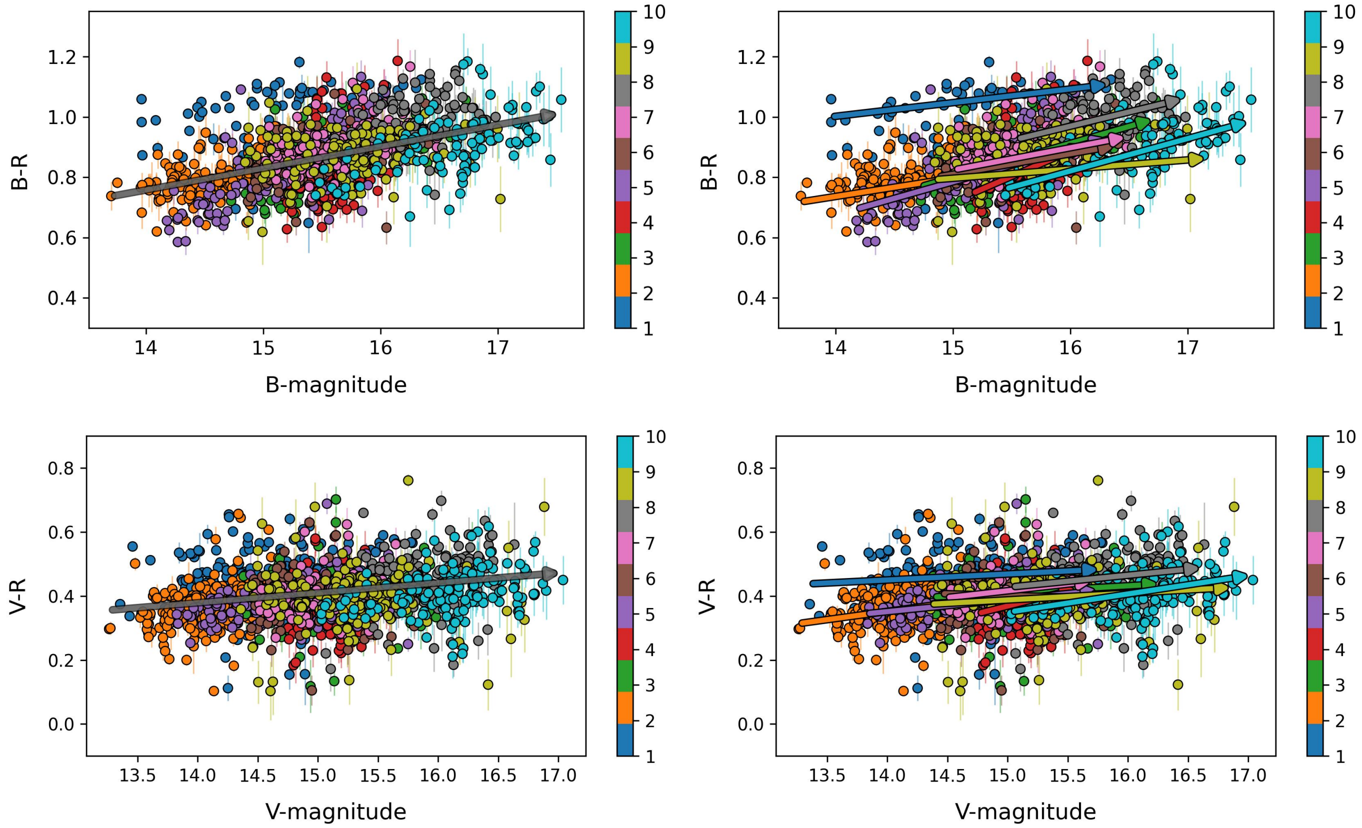

Figure 2. The left panels show the color–magnitude diagrams with a linear fit to all data points, whereas the right panels show the fit to all 10 segments.

Table 2
Total and Segment-wise Variability Amplitudes of OJ 287 from 2015-2025

	Band	V_{amp}		Band	V_{amp}		Band	V_{amp}
Segment 1	*B*	2.38 ± 0.01	Segment 2	*B*	1.88 ± 0.06	Segment 3	*B*	2.00 ± 0.06
	V	2.87 ± 0.02		*V*	2.08 ± 0.04		*V*	1.97 ± 0.04
	R	2.45 ± 0.02		*R*	2.57 ± 0.01		*R*	2.03 ± 0.03
	I	2.69 ± 0.02		*I*	1.79 ± 0.01		*I*	1.72 ± 0.02
Segment 4	*B*	1.11 ± 0.08	Segment 5	*B*	2.18 ± 0.06	Segment 6	*B*	1.56 ± 0.05
	V	0.91 ± 0.05		*V*	1.98 ± 0.04		*V*	1.42 ± 0.04
	R	0.96 ± 0.03		*R*	2.05 ± 0.02		*R*	1.58 ± 0.02
	I	0.86 ± 0.07		*I*	2.27 ± 0.03		*I*	1.45 ± 0.03
Segment 7	*B*	1.49 ± 0.02	Segment 8	*B*	1.48 ± 0.08	Segment 9	*B*	2.67 ± 0.10
	V	1.30 ± 0.08		*V*	1.75 ± 0.05		*V*	2.60 ± 0.07
	R	1.98 ± 0.03		*R*	1.84 ± 0.05		*R*	2.51 ± 0.11
	I	1.31 ± 0.02		*I*	1.41 ± 0.03		*I*	2.28 ± 0.09
Segment 10	*B*	2.10 ± 0.09	Total light curve	*B*	3.83 ± 0.09	…	…	…
	V	2.09 ± 0.07		*V*	4.13 ± 0.06	…	…	…
	R	2.25 ± 0.08		*R*	4.14 ± 0.07	…	…	…
	I	2.14 ± 0.08		*I*	4.22 ± 0.06	…	…	…

an equal number of data pairs, improving statistical reliability across all lag ranges. Let n be the number of (x_i, y_i) pairs in a given time-lag bin, then, for each bin, the correlation coefficient r is computed as

$$r = \frac{\sum_i^n (x_i - \bar{x})(y_i - \bar{y})/(n-1)}{s_x s_y}, \tag{3}$$

which is then transformed using Fisher's z-transformation:

$$z = \frac{1}{2}\log\left(\frac{1+r}{1-r}\right), \ \zeta = \frac{1}{2}\log\left(\frac{1+\rho}{1-\rho}\right), \ r = \tanh z. \tag{4}$$

Here $\bar{x}$, $\bar{y}$ are bin averages, s_x, s_y are their standard deviations, and ρ is the unknown population correlation coefficient of the

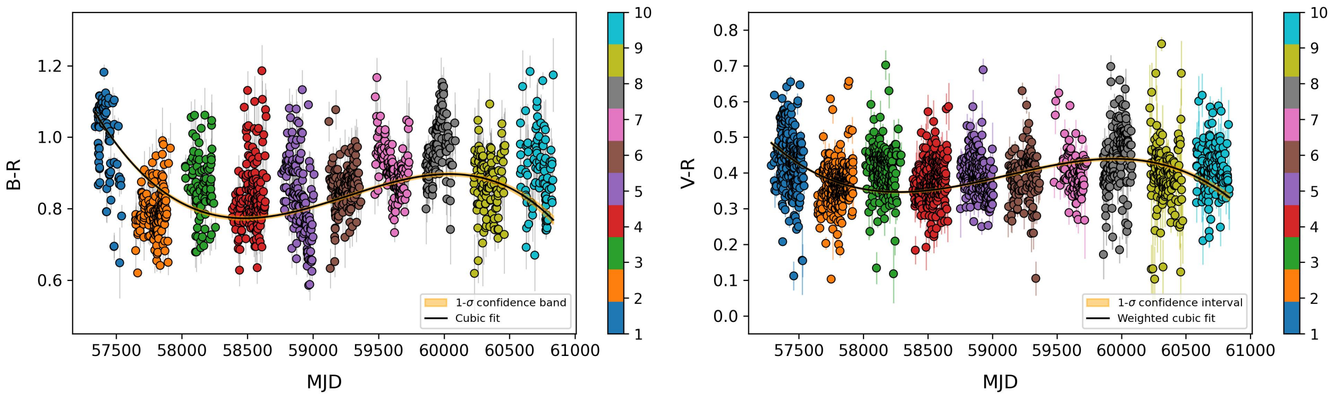

Figure 3. Color versus MJD plots for OJ 287. The plots show a slowly varying component, fitted with a cubic polynomial (in black).

Table 3
Fit Parameters for Color–Magnitude Diagrams

	$B-R$				$V-R$			
	Slope	Intercept	r	ρ	Slope	Intercept	r	ρ
Segment 1	0.0453 ± 0.0012	0.3677 ± 0.0171	0.312	0.405	0.0187 ± 0.0108	0.1878 ± 0.1557	0.105	0.092
Segment 2	0.0611 ± 0.0047	−0.1197 ± 0.0686	0.396	0.419	0.0516 ± 0.0102	−0.3706 ± 0.1436	0.256	0.296
Segment 3	0.1124 ± 0.0096	−0.8861 ± 0.1479	0.503	0.555	0.0216 ± 0.0095	0.0862 ± 0.1430	0.174	0.199
Segment 4	0.1686 ± 0.0081	−1.8098 ± 0.1262	0.339	0.317	0.0944 ± 0.0127	−1.0468 ± 0.1926	0.175	0.223
Segment 5	0.1102 ± 0.0040	−0.8682 ± 0.0597	0.710	0.717	0.0376 ± 0.0055	−0.1747 ± 0.0813	0.398	0.414
Segment 6	0.0679 ± 0.0060	−0.2077 ± 0.0915	0.337	0.387	−0.0103 ± 0.0130	0.5564 ± 0.1944	0.053	0.034
Segment 7	0.0739 ± 0.0046	−0.2846 ± 0.0718	0.408	0.509	0.0422 ± 0.0124	−0.2164 ± 0.1852	0.280	0.305
Segment 8	0.0945 ± 0.0091	−0.5427 ± 0.1472	0.330	0.363	0.0376 ± 0.0177	−0.1366 ± 0.2796	0.359	0.414
Segment 9	0.0304 ± 0.0063	0.3407 ± 0.0972	0.254	0.258	0.0209 ± 0.0087	0.0743 ± 0.1309	0.046	0.021
Segment 10	0.1076 ± 0.0050	−0.9001 ± 0.0823	0.570	0.594	0.0573 ± 0.0074	−0.5095 ± 0.1168	0.308	0.381
Total light curve	0.0720 ± 0.0042	−0.2500 ± 0.0502	0.479	0.495	0.0311 ± 0.0004	−0.0565 ± 0.0055	0.232	0.234

bin. Due to the presence of various emitting and absorbing regions surrounding an AGN, variations across different energy bands may not occur simultaneously, leading to observable time differences. To implement the ZDCF, we made use of the Python package `pyzdcf`[54] (I. Jankov et al. 2022). The results of the cross correlations are shown in Figure 4. As can be seen, the ZDCFs peak at zero lag, implying cospatial optical emission. The significance of the detected peaks are shown by red dashed lines in Figure 4 corresponding to a 3.5σ level. The significance is calculated by simulating 5×10^4 light curves, following the procedure discussed in D. Emmanoulopoulos et al. (2013).

These results are consistent with not only the optical–optical correlations, but between different bands as well, although sometimes lags of few days have been detected. For example, cross-correlation analyses have shown that optical and γ-ray light curves are often very closely aligned, with any lag mostly consistent with being zero or sometimes a few days (S. Vercellone et al. 2009; B. Rajput et al. 2019; G. Bhatta 2021). Such behavior tends to favor leptonic models where synchrotron emission and inverse-Compton scattering (γ-rays) come from the same lepton population, rather than more complex multizone or hadronic scenarios (E. W. Bonning et al. 2009; N. H. Liao et al. 2014; A. Majumder et al. 2019). Lags of the order of several to hundreds of days have also been observed, but these typically involve cross correlations between, e.g., lower-frequency radio and optical light curves (A. Sarkar et al. 2019).

4. Estimation of the Black Hole Mass in OJ 287 Using Steward Optical Spectra

We combined eight optical spectra of OJ 287 at its low state, in the observed period from 2017 October 21 to 2017 November 22, from Steward Observatory[55] with the observed wavelength range $\lambda = 4000$–7550 Å. All eight spectra and the flux-averaged spectrum are plotted in the left panel of Figure 5. There are no significant emission lines in the individual spectra, but a weak [O III] line appears at 5007 Å in the average spectrum indicated by the blue dotted lines in both panels. As neither broad-emission lines nor the host absorption lines are observed in the average spectrum, the virial mass and M–σ empirical relation estimations cannot be directly applied to obtain the BH mass for OJ 287.

However, we can employ the [O III] line width to estimate the BH mass. The width of narrow-line [O III] has frequently been used as a surrogate for σ because the bulge gravity dominates the global kinematics of the narrow-line region in AGNs (e.g., S. Komossa & D. Xu 2007; Q. Wu 2009, and references therein). We analyzed the average spectrum following the procedure given in M. Liao & M. Gu (2020), where the average spectrum was first corrected for Galactic

[54] https://github.com/LSST-sersag/pyzdcf

[55] http://james.as.arizona.edu/~psmith/Fermi

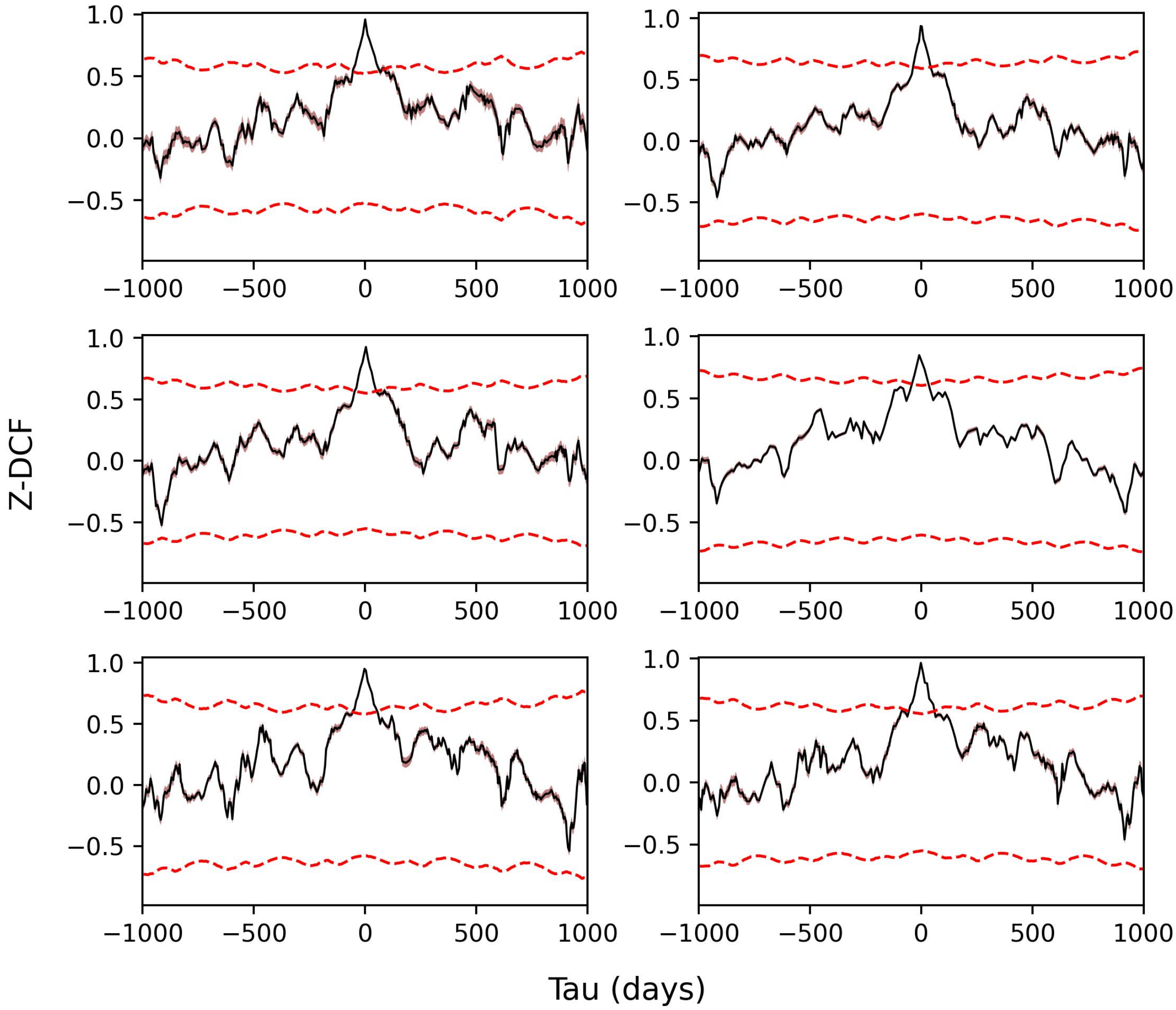

Figure 4. Cross-correlation results between different optical bands. With all ZDCFs peaking at zero lag, one can infer essentially cospatial emission, with the red dashed line representing 3.5σ significance level.

extinction with the reddening map of D. J. Schlegel et al. (1998), and then was shifted to the rest-frame wavelength by using the redshift of OJ 287. We modeled the continuum by applying a single power law ($f_\lambda \propto \lambda^\alpha$). The continuum-subtracted average spectrum was further fitted by using the Gaussian profile to fit the [O III] λ5007 Å in the spectral range of 4700–5100 Å. The final full width at half-maximum (FWHM) of [O III] is 841 km s^{-1}, which was corrected for instrumental line broadening with the adopted source-frame instrumental resolution of FWHM$_{\rm instr} \simeq$ 918 km s^{-1}. In order to evaluate the corresponding error of FWHM, we generated 100 mock spectra by adding a random Gaussian noise to the original spectra using the flux-density errors, and then calculated the standard deviation of the measurements from those mock spectra as the uncertainty. The flux-density errors used here were the rms value of the average spectrum calculated over the source-frame spectral window of 5100 −5150 Å after subtracting a second-order polynomial function. The spectral fitting is shown in the right panel of Figure 5.

Using the M–σ relation of J. Kormendy & L. C. Ho (2013) where σ = FWHM$_{\rm [O\ III]}$/2.35, we estimated the BH mass to be log ($M_{\rm BH}/M_\odot$)= 9.59. The systematic uncertainty of the M–σ relation of 0.29 dex has been combined with the [O III]-based FWHM (0.27 dex) to produce a total error for this BH mass estimate, yielding log ($M_{\rm BH}/M_\odot$) = 9.59 ± 0.40. So the BH mass from this initial [O III] estimate could be up to 10 × 10^9 $M_\odot$, which is comparable to that derived from the binary model for the massive one of $M_{\rm BH}$ = 18.35 ± 0.05 × 10^9 $M_\odot$ (M. J. Valtonen 2007). The [O III] emission line is from the AGN narrow-line emission region at the kiloparsecs scale, which is generally believed to be a cone structure rather than a disk; therefore, the projection effect may not be as important as when one considers the broad line region (BLR). The preferred lines for BH mass estimates, H$_\alpha$ and H$_\beta$ are from the BLR, which is located much closer to the BH than the narrow-line emission region. There is another source of uncertainty which, while alluded to, is yet to be included. Since the line-emitting region is likely to be geometrically flat, and lie close to the plane of the sky in BL Lac objects such as OJ 287, the observed line width is narrower than it should be in comparison with an arbitrary viewing angle by a factor sin i where i is the inclination of the disk. Ideally, one would use an experimental M–σ relation for BL Lac objects, but since it is not available, the best we can do

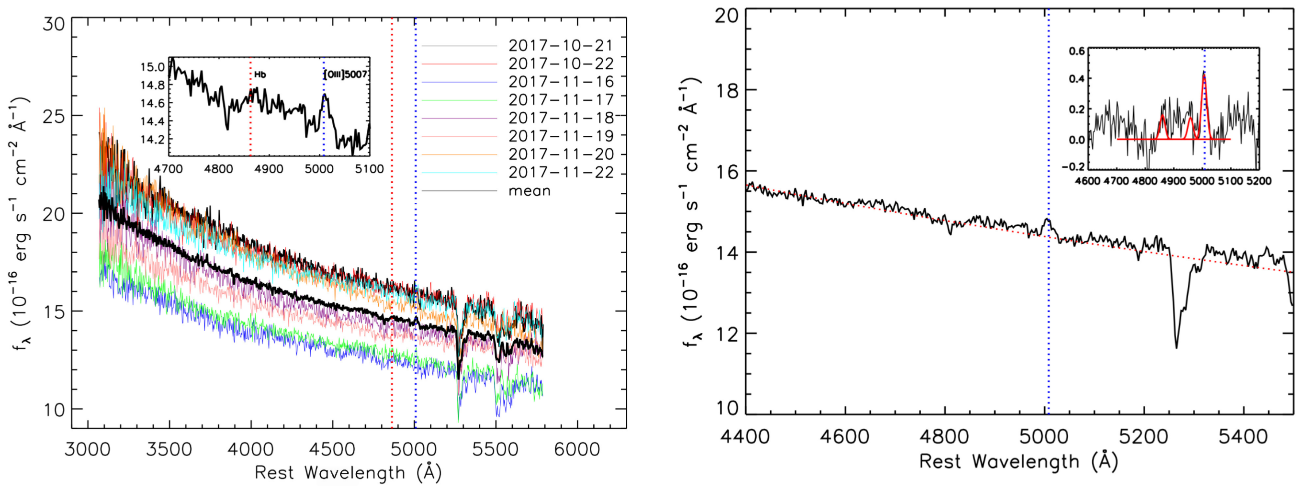

Figure 5. The eight spectra observed in the period of 2017 October 21–2017 November 22 and the flux-averaged spectrum (left). All spectra were corrected for Galactic extinction and shifted to source rest frame, with the position of emission lines of Hβ and [O III] λ5007 Å indicated as the vertical red dotted and green dotted lines. The spectral fitting of OJ 287 (right), where the continuum is fitted with a single power law shown as the red dotted line; the black line is the original flux-averaged spectrum and the inset shows the line fitting for [O III] λ5007 Å.

is to estimate the influence of the sin i factor on the determined BH mass value. The correction factor could be up to a factor of 10 for the narrow-line region, so we can only say that the value of the BH mass mentioned above is a lower limit. The dynamically determined mass from the binary motion log $(M/M_\odot) = 10.25$ (M. J. Valtonen 2007) is certainly compatible with this limit.

We note that S. Komossa et al. (2023a) refer to M. Vestergaard & B. M. Peterson (2006) who derived a correlation between the BH mass $M_{\rm BH}$ and the hydrogen line luminosity $L({\rm H}_\beta)$ (in units of 10^{42} erg s^{-1}) and the line width at half-maximum $F({\rm H}_\beta)$ (in units of 1000 km s^{-1}) in quasars:

$$M_{\rm BH} = 10^{6.67}\,[L({\rm H}_\beta)]^{0.63}\,[F({\rm H}_\beta)]^2 M_\odot. \quad (5)$$

They use the line parameters measured in 1984 December 23 by M. L. Sitko & V. T. Junkkarinen (1985) $L({\rm H}_\alpha) = 10^{42.8}$ erg s^{-1} and $F({\rm H}_\alpha) = 4200$ km s^{-1} and obtain the BH mass of only $M_{\rm BH} \sim 1.25 \times 10^8 M_\odot$. They ignore the influence of the disk's inclination. The inclination of the accretion disk with respect to the plane of the sky i is likely to be low in OJ 287, say $i \sim 5^\circ$, because the jet is pointing nearly in our direction. The Doppler broadening should be proportional to sin i, if the BLR is flattened. Comparing this with a typical value of $(\sin i)^{-1}$ in a randomly oriented sample, this correction factor for OJ 287 would be around 10, increasing the estimated mass by a factor of 10^2 over the correlation value. Therefore, after the inclination correction, the mass estimate of S. Komossa et al. (2023a) is consistent with what we find from the [O III] line, as well as the binary-SMBH dynamical measurement.

Now the binary-SMBH model is based on the long-term quasiperiodic variability of the source, interpreted as the result of orbital motion and disk-impact events. Recent radio and MW studies (e.g., A. Volvach et al. 2024, 2025) have identified multiple stable periodic components (of ∼12, ∼6.5, and ∼2.1 yr), which are naturally explained within a binary framework and produce additional direct constraints on the system's dynamical parameters. These analyses suggest a primary BH mass of $\sim 10^{10} M_\odot$ and a secondary component of $\sim 10^9 M_\odot$, consistent with the dynamically determined mass from the long-term optical observations (e.g., M. J. Valtonen 2007).

Therefore, the lower mass derived from the M–σ relation should be regarded as a conservative estimate, while the dynamically inferred mass from the binary model is most likely more representative of the true gravitational potential of the system. This is particularly relevant for OJ 287, where relativistic jet emission dominates and can significantly affect spectroscopic diagnostics. The comparison highlights the importance of combining spectroscopic and time-domain approaches when studying complex systems such as blazars hosting candidate binary SMBHs.

5. Discussion

Here, we have investigated approximately 10 yr of densely sampled multiband optical observations of OJ 287, spanning from 2015 September 29 to 2025 April 26. The dataset was compiled from an extensive network of telescopes worldwide, yielding the most densely sampled light curve of the source to date. It incorporates both previously published observations (A. C. Gupta et al. 2017, 2019, 2023) and newly obtained data provided by our collaborators. Additionally, publicly available data from the SMARTS and Steward observatories were included to further enhance the dataset's temporal coverage and reliability. Due to seasonal gaps, we divided the light curve into 10 distinct segments. All segments exhibit noticeable variability across all bands; however, the amplitude of variation differs significantly between them. Segment 1 (corresponding to 2015/6) shows the greatest variability, with brightness changes of approximately 2.7 mag, suggesting a phase of strong activity. In contrast, segment 4 (2018/9) shows the least variation, with a relatively modest change of ∼1 mag, illustrating a comparatively stable emission state.

OJ 287 is a remarkable blazar that certainly appears to host a binary-SMBH system, where the secondary periodically impacts the accretion disk of the primary roughly every 12 yr (H. J. Lehto & M. J. Valtonen 1996; A. Sillanpaa et al. 1996b; M. J. Valtonen et al. 2008). This periodic interaction produces characteristic optical outbursts, although none were captured in the present analysis, as our observational baseline is a few years shorter than the expected period.

Blazar flux variability spans a wide range of timescales and can arise from both accretion-disk instabilities (S. A. Balbus & J. F. Hawley 1991; Y. E. Lyubarskii 1997; P. Arévalo & P. Uttley 2006) and jet-dynamics-driven processes. The former can lead to small-scale amplitude variations either due to instabilities in the accretion disk or by a change in accretion rate near the inner edge of the disk. Among the latter, the shock-in-jet model (A. P. Marscher & W. K. Gear 1985) provides a natural explanation for many large flares in many wave bands, where shocks propagating along the relativistic jet accelerate particles and enhance synchrotron emission. The resulting emission can either predominantly originate from a single zone (G. Ghisellini et al. 1998; F. Tavecchio et al. 1998), or seems to require contributions from multiple zones (X. Chen et al. 2011; A. P. Marscher 2014). Collisions between stationary and traveling shocks within the jet give rise to multiple radiation zones and are used to explain the short-term MW variability; meanwhile, the single zone models are helpful in explaining the long-term variability since the finite size of the emission region and the associated light-crossing time, along with particle injection timescales, naturally predict a larger minimum timescale for flaring episodes (e.g., K. K. Singh & P. J. Meintjes 2020). Geometrical effects can also play a key role in observed variability by affecting the bulk Lorentz factor, which in turn can increase or decrease the observed flux (C. M. Raiteri et al. 2017b; A. Sarkar et al. 2019).

Blazars typically exhibit two main types of color behavior: RWB and BWB trends. As a blazar, and specifically a BL Lac object in which quasi-thermal accretion-disk emission is minimal, the variability of OJ 287 is primarily driven by the jet emission. In the case of BL Lac objects, most studies point toward a dominant BWB trend (M. F. Gu et al. 2006; Y.-H. Zhang et al. 2013). In this work, we analyzed the long-term color variability of OJ 287 and found a clear BWB trend, not only in the full light curve, but also consistently across all 10 individual segments. The BWB trend seen in BL Lac objects can be attributed to electrons accelerated by the shock front in the jet losing energy more quickly, leading to greater variability in the higher-energy bands (A. Mastichiadis & J. G. Kirk 2002). Alternatively, the rise in luminosity could be explained by the injection of new electrons with a harder energy distribution compared to the previously cooled population.

Since the confirmation of the large precession in the binary orbit and the detection of loss of the gravitational-wave energy from the system (M. J. Valtonen et al. 2008), the interest in MW observations has boomed. In particular, the predicted 2015 flare was already much better covered observationally than the previous flares that mark the binary orbit (M. J. Valtonen et al. 2016). This could be considered the start of the high MW observational efforts. As far as we know, the spectral and temporal behavior has not been any different from earlier flaring periods, but the coverage has improved (P. Kushwaha et al. 2018a, 2018b). The dynamic evolution of the emission from OJ 287, backed by a certain predictability, rare in a transient dynamical system, has encouraged a great deal of MW monitoring. Investigations of these accumulated rich datasets have led to the discovery of many new features including a thermal spectral component in the NIR-optical band (P. Kushwaha et al. 2018b); an additional high-synchrotron-peaked BL Lac object–like jet-emission component (S. O. Brien & VERITAS Collaboration 2017; P. Kushwaha et al. 2018a, 2021; K. P. Singh et al. 2022), with an unusually soft-X-ray spectrum (S. Komossa et al. 2017, 2020; P. Kushwaha et al. 2018b, 2021; B. Kapanadze et al. 2018; S. Huang et al. 2021); a Seyfert-like UV and soft-X-ray excess (M. Pal et al. 2020); an iron absorption feature (S. Komossa et al. 2020); systematic trends in optical polarization (M. H. Cohen et al. 2018; A. C. Gupta et al. 2019, 2023); and secondary jets (E. Bonnassieux et al. 2024; M. J. Valtonen et al. 2025), most of these for the first time. Interestingly and intriguingly, all of these newer, peculiar features are detected when the two SMBHs are closely interacting as per the dynamical evolution of the disk-impact model. These, in turn, has further expanded the scope of observations and now OJ 287 is one of the targets of the Event Horizon Telescope (EHT; I. Cho et al. 2024).

These fascinating findings in turn have greatly enlarged the physics of this source that can be probed, apart from binary aspects. These include strong gravity physics involving tidal disruptions (S. Huang et al. 2021); BH properties (e.g., M. J. Valtonen et al. 2008, 2023; A. C. Gupta et al. 2023, and references therein); gravitational waves (e.g., M. J. Valtonen et al. 2008; J.-W. Chen & Y. Zhang 2018; G. Agazie et al. 2023, and references therein); accretion and aspects of relativistic jets (e.g., S. Komossa et al. 2020; A. C. Gupta et al. 2022, 2023; P. Kushwaha 2025, 2022; S. M. Ressler et al. 2025, and references therein); aspects of cosmology (e.g., M. H. Chan & C. M. Lee 2024; S. Yadav & P. Kushwaha 2024; D. Deb et al. 2025); and finally, as a multimessenger source (e.g., J. C. Rodríguez-Ramírez et al. 2020; M. J. Valtonen et al. 2021).

6. Conclusions

This study presents densely sampled investigations of the long-term optical variability of the blazar OJ 287. The analysis is based on an extensive collection of optical photometric observations acquired from numerous ground-based telescopes worldwide, covering its emission as continuously as possible from the ground between 2015 and 2025. A concise summary of our main results is provided below.

1. Due to the seasonal gaps, the light was divided into a total of 10 segments, with the object going through a maximum and minimum magnitude change of ∼2.87 and 0.86 in the V band (segment 1) and I band (segment 4), respectively. The object was found to be variable throughout the observing campaign, but faded steadily after the peak of the 2015 disk-impact flare, reaching $V = 16.86$ in April 2025.
2. The CM relationship for OJ 287 was analyzed both over the entire light curve and across individual segments. A clear "bluer-when-brighter" trend was observed, not only in the full light curve, but also consistently within each segment. Among the $B - R$ color indices, the strongest and weakest correlations were found in segments 5 (2019/2020) and 9 (2023/2024), with Spearman correlation coefficients, ρ, of 0.717 and 0.258, respectively. For the full light curve, Spearman ρ was 0.495.
3. The discrete correlation function analysis was performed between all bands using ZDCF. All interband cross correlations were found to peak at zero lag, implying that the emission is cospatial in the BVRI bands.
4. We combined eight optical spectra of the source to estimate its BH mass by using the width of the [O III] line as a surrogate for σ in the M–σ relation. The continuum

was fitted using a power law, while the continuum-subtracted average spectrum was fitted using a Gaussian function, giving a $\mathrm{FWHM}_{\mathrm{instru}} \simeq 918\ \mathrm{km\,s^{-1}}$ which translates to a BH mass of $\log M_{\mathrm{BH}} = 9.59 \pm 0.40 M_{\odot}$. This should be considered as the lower limit for the mass of the primary BH; it is consistent with the dynamically determined mass of $\log(M/M_{\odot}) = 10.25$.

Acknowledgments

We are sad to note that V. M. Larionov, R. Pickard, and E. Semkov passed away during this extended observation campaign. They were dedicated collaborators, and their contributions to our team will be greatly missed. We thankfully acknowledge the contribution by V. M. Larionov, who is not included as a coauthor of the paper at the suggestion of his family.

Data from the Steward Observatory spectropolarimetric monitoring project were used. This program is supported by Fermi Guest Investigator grants NNX08AW56G, NNX09AU10G, NNX12AO93G, and NNX15AU81G. This paper has made use of up-to-date SMARTS optical/near-IR light curves that are available.[56]

We thank the anonymous reviewer for constructive comments. This work was supported by the Tianshan Talent Training Program with grant No. 2023TSYCCX0099. A.C.G. is partially supported by the CAS "President's International Fellowship Initiative (PIFI)" with grant No. 2026PVA0040. The Abastumani team acknowledges financial support by the Shota Rustaveli NSF of Georgia under contract FR-24-515. P.K. acknowledges support from the Department of Science and Technology (DST), government of India, through the DST-INSPIRE Faculty grant (DST/INSPIRE/04/2020/002586). The research at Boston University was supported in part by several NASA Fermi Guest Investigator grants, the latest is 80NSSC26K0222. This study was based in part on observations conducted using the 1.8 m Perkins Telescope Observatory (PTO) in Arizona, which is owned and operated by Boston University. K.M. acknowledges support from JSPS KAKENHI grant number 19K03930. The work of S.M.H. and X.C. is supported by the National Natural Science Foundation of China under grant No. 12373015. G.D., O.V., M.S. and M.D.J. acknowledge support by the Astronomical Station Vidojevica and the Ministry of Science, Technological Development and Innovation of the Republic of Serbia (MSTDIRS) through contract no. 451-03-33/2026-03/200002 made with Astronomical Observatory (Belgrade), by the EC through project BELISSIMA (call FP7-REGPOT-2010-5, No. 256772), the observing and financial grant support from the Institute of Astronomy and Rozhen NAO BAS through the bilateral SANU-BAN joint research projects "Astrometric and astrophysical research of variable astronomical objects," and "Optical flux stability of 47 Active Galactic Nuclei important for the link between the Gaia CRF and ICRF systems," and support by the SANU project F-187. Also, this research was supported by the Science Fund of the Republic of Serbia, grant no. 6775, Urban Observatory of Belgrade—UrbObsBel, and grant no. 7337 (Modeling Binary Systems That End in Stellar Mergers and Give Rise to Gravitational Waves—MOBY). This research was partially supported by the Bulgarian National Science Fund of the Ministry of Education and Science under grant KP-06-H88/4 (2024). M.L. is supported by the grants from the Rubin-Chile Fund (DIA3324). J.H.F.'s work is partially supported by the National Natural Science Foundation of China (NSFC grant 12433004) and grant 2025YFA1614102. H.G. acknowledges financial support from the Department of Science & Technology, India through INSPIRE faculty award IFA17-PH197 at ARIES, Nainital. M.F.G. is supported by the National Science Foundation of China (grant 12473019), the Shanghai Pilot Program for Basic Research-Chinese Academy of Science, Shanghai Branch (JCYJ-SHFY-2021-013), the National SKA Program of China (grant No. 2022SKA0120102), the National Science and Technology Major Project (2024ZD1100601), and the China Manned Space Project with No. CMS-CSST-2025-A07. B.V. is funded by the Swedish Research Council (Vetenskapsrådet, grant no. 2017-06372). Z.Z. is thankful for support from the National Key R&D Programme of China (under grant no. 2018FA0404602) and the Chinese Academy of Sciences (CAS) for the Talented Program. W.Z. is supported by the Shanghai Natural Science Foundation Youth Project 25ZR1402546, and Strategic Priority Research Program of the Chinese Academy of Sciences (CAS) grant No. XDB0800302.

Data Availability

Data may be provided on a reasonable request to A.C.G. or K.D.

ORCID iDs

Alok C. Gupta https://orcid.org/0000-0002-9331-4388
Karan Dogra https://orcid.org/0009-0007-3214-602X
Mauri J. Valtonen https://orcid.org/0000-0001-8580-8874
Paul J. Wiita https://orcid.org/0000-0002-1029-3746
Pankaj Kushwaha https://orcid.org/0000-0001-6890-2236
Sergey S. Savchenko https://orcid.org/0000-0003-4147-3851
Sofia O. Kurtanidze https://orcid.org/0000-0002-0319-5873
Svetlana G. Jorstad https://orcid.org/0000-0001-6158-1708
Alan P. Marscher https://orcid.org/0000-0001-7396-3332
Katsura Matsumoto https://orcid.org/0000-0002-5277-568X
Lang Cui https://orcid.org/0000-0003-0721-5509
Shao Ming Hu https://orcid.org/0000-0003-3217-7794
Goran Damljanovic https://orcid.org/0000-0002-6710-6868
Rumen Bachev https://orcid.org/0000-0002-0766-864X
O. Vince https://orcid.org/0009-0008-5761-3701
Mai Liao https://orcid.org/0000-0002-9137-7019
Zhongxiang Wang https://orcid.org/0000-0003-1984-3852
S. Haque https://orcid.org/0000-0002-9158-7091
G. A. Borman https://orcid.org/0000-0002-7262-6710
X. Chen https://orcid.org/0000-0001-5603-7521
P. U. Devanand https://orcid.org/0000-0003-3337-4861
V. Dhiman https://orcid.org/0000-0002-8105-4566
J. H. Fan https://orcid.org/0000-0002-5929-0968
H. Gaur https://orcid.org/0000-0002-6629-8490
T. S. Grishina https://orcid.org/0000-0002-3953-6676
M. F. Gu https://orcid.org/0000-0002-4455-6946
H. Guo https://orcid.org/0000-0001-8416-7059
V. A. Hagen-Thorn https://orcid.org/0000-0002-6431-8590
S. Ibryamov https://orcid.org/0000-0002-4618-1201
R. Z. Ivanidze https://orcid.org/0009-0005-7297-8985
B. Jardine https://orcid.org/0009-0005-3426-5394
M. D. Jovanovic https://orcid.org/0000-0003-4298-3247
N. Kalita https://orcid.org/0000-0002-9323-4150

[56] http://www.astro.yale.edu/smarts/glast/home.php

S. Kishore https://orcid.org/0000-0001-8716-9412
E. N. Kopatskaya https://orcid.org/0000-0001-9518-337X
O. M. Kurtanidze https://orcid.org/0000-0001-5385-0576
E. G. Larionova https://orcid.org/0000-0002-2471-6500
D. A. Morozova https://orcid.org/0000-0002-9407-7804
M. G. Nikolashvili https://orcid.org/0000-0003-0408-7177
P. A. Novikova https://orcid.org/0009-0002-9081-5563
F. Rahmatullaeva https://orcid.org/0009-0002-1610-6136
B. Rajkumar https://orcid.org/0000-0002-2227-9749
E. V. Shishkina https://orcid.org/0009-0002-2440-2947
M. Stojanovic https://orcid.org/0000-0002-4105-7113
T. Tripathi https://orcid.org/0009-0006-3586-2489
Yu. V. Troitskaya https://orcid.org/0000-0002-9907-9876
I. S. Troitskiy https://orcid.org/0000-0002-4218-0148
A. A. Vasilyev https://orcid.org/0000-0002-8293-0214
B. Villarroel https://orcid.org/0000-0002-4101-237X
A. E. Volvach https://orcid.org/0000-0002-3839-3466
L. N. Volvach https://orcid.org/0000-0001-6157-003X
S. J. Wagner https://orcid.org/0000-0002-7474-6062
Z. R. Weaver https://orcid.org/0000-0001-6314-0690
Wen-Xin Yang https://orcid.org/0009-0008-3069-3975
Z. Zhang https://orcid.org/0000-0002-8366-3373
W. Zuo https://orcid.org/0000-0002-4521-6281

References

Abdo, A. A., Ackermann, M., Agudo, I., et al. 2010, ApJ, 716, 30
Agazie, G., Anumarlapudi, A., Archibald, A. M., et al. 2023, ApJL, 951, L8
Alexander, T. 1997, ASSL, 218, 163
Arévalo, P., & Uttley, P. 2006, MNRAS, 367, 801
Balbus, S. A., & Hawley, J. F. 1991, ApJ, 376, 214
Bhatta, G. 2021, ApJ, 923, 7
Bhatta, G., Zola, S., Stawarz, Ł., et al. 2016, ApJ, 832, 47
Bonnassieux, E., Shetgaonkar, H., & Kadler, M. 2024, SF2A-2024: Proc. of the Annual Meeting of the French Society of Astronomy and Astrophysics, ed. M. Béthermin et al., 377
Bonning, E., Urry, C. M., Bailyn, C., et al. 2012, ApJ, 756, 13
Bonning, E. W., Bailyn, C., Urry, C. M., et al. 2009, ApJL, 697, L81
Brien, S. O. & VERITAS Collaboration 2017, ICRC, 301, 650
Britzen, S., Zajaček, M., Gopal-Krishna, et al. 2023, ApJ, 951, 106
Britzen, S., Fendt, C., Witzel, G., et al. 2018, MNRAS, 478, 3199
Butuzova, M. S., & Pushkarev, A. B. 2020, Univ, 6, 191
Chan, M. H., & Lee, C. M. 2024, ApJL, 962, L40
Chen, J.-W., & Zhang, Y. 2018, MNRAS, 481, 2249
Chen, X., Fossati, G., Liang, E. P., & Böttcher, M. 2011, MNRAS, 416, 2368
Cho, I., Gómez, J. L., Lico, R., et al. 2024, A&A, 683, A248
Cohen, M. H., Aller, H. D., Aller, M. F., et al. 2018, ApJ, 862, 1
de Naurois, M. 2021, Univ, 7, 421
Deb, D., Gopakumar, A., & Valtonen, M. J. 2025, ApJL, 984, L66
Di Gesu, L., Marshall, H. L., Ehlert, S. R., et al. 2023, NatAs, 7, 1245
Dogra, K., Gupta, A. C., Raiteri, C. M., et al. 2025, ApJS, 276, 1
Edelson, R. A., & Krolik, J. H. 1988, ApJ, 333, 646
Emmanoulopoulos, D., McHardy, I. M., & Papadakis, I. E. 2013, MNRAS, 433, 907
Fossati, G., Maraschi, L., Celotti, A., Comastri, A., & Ghisellini, G. 1998, MNRAS, 299, 433
Gao, S., Fedynitch, A., Winter, W., & Pohl, M. 2019, NatAs, 3, 88
Ghisellini, G., Celotti, A., Fossati, G., Maraschi, L., & Comastri, A. 1998, MNRAS, 301, 451
Giesers, B., Dreizler, S., Husser, T.-O., et al. 2018, MNRAS, 475, L15
González-Pérez, J. N., Kidger, M. R., & Martín-Luis, F. 2001, AJ, 122, 2055
Gopal-Krishna 2024, A&A, 688, L16
Goyal, A., Stawarz, Ł., Zola, S., et al. 2018, ApJ, 863, 175
Gu, M. F., & Ai, Y. L. 2011, A&A, 528, A95
Gu, M. F., Lee, C. U., Pak, S., Yim, H. S., & Fletcher, A. B. 2006, A&A, 450, 39
Gupta, A. C., Agarwal, A., Mishra, A., et al. 2017, MNRAS, 465, 4423
Gupta, A. C., Gaur, H., Wiita, P. J., et al. 2019, AJ, 157, 95
Gupta, A. C., Kushwaha, P., Carrasco, L., et al. 2022, ApJS, 260, 39
Gupta, A. C., Kushwaha, P., Valtonen, M. J., et al. 2023, ApJL, 957, L11
Harutyunyan, G., Sahakyan, N., & Bégué, D. 2025, MNRAS, 540, 582
Huang, S., Hu, S., Yin, H., et al. 2021, ApJ, 920, 12
Imazawa, R., Sasada, M., Hazama, N., et al. 2023, PASJ, 75, 1
Isobe, N., Tashiro, M., Sugiho, M., & Makishima, K. 2001, PASJ, 53, 79
Jankov, I., Kovačević, A. B., Ilić, D., Sánchez-Sáez, P., & Nikutta, R. 2022, pyZDCF: Initial Release, v1.0.0, Zenodo, doi:10.5281/zenodo.7253034
Kapanadze, B., Vercellone, S., Romano, P., et al. 2018, MNRAS, 480, 407
Kishore, S., Gupta, A. C., & Wiita, P. J. 2024, ApJ, 960, 11
Komossa, S., Grupe, D., Gallo, L. C., et al. 2021a, ApJ, 923, 51
Komossa, S., Grupe, D., Kraus, A., et al. 2021b, Univ, 7, 261
Komossa, S., Grupe, D., Kraus, A., et al. 2023a, MNRAS, 522, L84
Komossa, S., Grupe, D., Parker, M. L., et al. 2020, MNRAS, 498, L35
Komossa, S., Grupe, D., Parker, M. L., et al. 2021c, MNRAS, 504, 5575
Komossa, S., Grupe, D., Schartel, N., et al. 2017, IAUS, 324, 168
Komossa, S., Kraus, A., Grupe, D., et al. 2023b, ApJ, 944, 177
Komossa, S., & Xu, D. 2007, ApJ, 667, L33
Kormendy, J., & Ho, L. C. 2013, ARA&A, 51, 511
Kushwaha, P. 2020, Galax, 8, 15
Kushwaha, P. 2022, JApA, 43, 79
Kushwaha, P. 2025, Univ, 11, 84
Kushwaha, P., Gupta, A. C., Wiita, P. J., et al. 2018a, MNRAS, 479, 1672
Kushwaha, P., Gupta, A. C., Wiita, P. J., et al. 2018b, MNRAS, 473, 1145
Kushwaha, P., Pal, M., Kalita, N., et al. 2021, ApJ, 921, 18
Kushwaha, P., Sahayanathan, S., & Singh, K. P. 2013, MNRAS, 433, 2380
Laine, S., Dey, L., Valtonen, M., et al. 2020, ApJL, 894, L1
Lehto, H. J., & Valtonen, M. J. 1996, ApJ, 460, 207
Liao, M., & Gu, M. 2020, MNRAS, 491, 92
Liao, N. H., Bai, J. M., Liu, H. T., et al. 2014, ApJ, 783, 83
Lyubarskii, Y. E. 1997, MNRAS, 292, 679
MAGIC Collaboration, Abe, H., Abe, S., et al. 2024, A&A, 682, A114
Majumder, A., Mitra, K., Chatterjee, R., et al. 2019, MNRAS, 490, 124
Marscher, A. P. 2014, ApJ, 780, 87
Marscher, A. P., & Gear, W. K. 1985, ApJ, 298, 114
Mastichiadis, A., & Kirk, J. G. 2002, PASA, 19, 138
Navaneeth, P. K., Bhatta, G., & Kizhakkekalam, S. 2025, MNRAS, 544, 2455
Nilsson, K., Takalo, L. O., Lehto, H. J., & Sillanpää, A. 2010, A&A, 516, A60
Pal, M., Kushwaha, P., Dewangan, G. C., & Pawar, P. K. 2020, ApJ, 890, 47
Prandini, E., & Ghisellini, G. 2022, Galax, 10, 35
Prince, R., Agarwal, A., Gupta, N., et al. 2021, A&A, 654, A38
Raiteri, C. M., Nicastro, F., Stamerra, A., et al. 2017a, MNRAS, 466, 3762
Raiteri, C. M., Villata, M., Acosta-Pulido, J. A., et al. 2017b, Natur, 552, 374
Raiteri, C. M., Villata, M., Jorstad, S. G., et al. 2023, MNRAS, 522, 102
Raiteri, C. M., Villata, M., Larionov, V. M., et al. 2008, A&A, 491, 755
Rajput, B., Stalin, C. S., Sahayanathan, S., Rakshit, S., & Mandal, A. K. 2019, MNRAS, 486, 1781
Ressler, S. M., Combi, L., Ripperda, B., & Li, X. 2025, ApJL, 993, L22
Rodríguez-Ramírez, J. C., Kushwaha, P., de Gouveia Dal Pino, E. M., & Santos-Lima, R. 2020, MNRAS, 498, 5424
Sarkar, A., Chitnis, V. R., Gupta, A. C., et al. 2019, ApJ, 887, 185
Schlegel, D. J., Finkbeiner, D. P., & Davis, M. 1998, ApJ, 500, 525
Seta, H., Isobe, N., Tashiro, M. S., et al. 2009, PASJ, 61, 1011
Sillanpaa, A., Haarala, S., Valtonen, M. J., Sundelius, B., & Byrd, G. G. 1988, ApJ, 325, 628
Sillanpaa, A., Takalo, L. O., Pursimo, T., et al. 1996a, A&A, 305, L17
Sillanpaa, A., Takalo, L. O., Pursimo, T., et al. 1996b, A&A, 315, L13
Singh, K. K., & Meintjes, P. J. 2020, AN, 341, 713
Singh, K. P., Kushwaha, P., Sinha, A., et al. 2022, MNRAS, 509, 2696
Sitko, M. L., & Junkkarinen, V. T. 1985, PASP, 97, 1158
Smith, P. S., Montiel, E., Rightley, S., et al. 2009, arXiv:0912.3621
Tavecchio, F., Maraschi, L., & Ghisellini, G. 1998, ApJ, 509, 608
Valtonen, M. J. 2007, ApJ, 659, 1074
Valtonen, M. J., Dey, L., Gopakumar, A., et al. 2021, Galax, 10, 1
Valtonen, M. J., Dey, L., Zola, S., et al. 2025, ApJ, 992, 110
Valtonen, M. J., Lehto, H. J., Nilsson, K., et al. 2008, Natur, 452, 851
Valtonen, M. J., Lehto, H. J., Sillanpää, A., et al. 2006, ApJ, 646, 36
Valtonen, M. J., Zola, S., Ciprini, S., et al. 2016, ApJL, 819, L37
Valtonen, M. J., Zola, S., Gopakumar, A., et al. 2023, MNRAS, 525, 1153
Vercellone, S., Chen, A. W., Vittorini, V., et al. 2009, ApJ, 690, 1018
Vestergaard, M., & Peterson, B. M. 2006, ApJ, 641, 689
Villforth, C., Nilsson, K., Heidt, J., et al. 2010, MNRAS, 402, 2087
Volvach, A., Volvach, L., & Larionov, M. 2024, iSci, 27, 109427
Volvach, A., Volvach, L., & Larionov, M. 2025, ApJ, 992, 60
Wierzcholska, A., Ostrowski, M., Stawarz, Ł., Wagner, S., & Hauser, M. 2015, A&A, 573, A69
Wu, Q. 2009, MNRAS, 398, 1905
Yadav, S., & Kushwaha, P. 2024, Galax, 12, 34
Zhang, Y.-H., Bian, F.-Y., Li, J.-Z., & Shang, R.-C. 2013, MNRAS, 432, 1189